OPEN ACCESS
IOP PUBLISHING
ADVANCES IN NATURAL SCIENCES: NANOSCIENCE AND NANOTECHNOLOGY
Adv. Nat. Sci.: Nanosci. Nanotechnol. **4** (2013) 025004 (10pp)
doi:10.1088/2043-6262/4/2/025004

Hydrogen storage in Ti–TiO_2 multilayers*

Z Tarnawski[1], Nhu-T H Kim-Ngan[2], K Zakrzewska[3], K Drogowska[1,4], A Brudnik[3], A G Balogh[4], R Kužel[5], L Havela[5] and V Sechovsky[5]

[1] Faculty of Physics and Applied Computer Science, AGH University of Science and Technology, 30-059 Kraków, Poland
[2] Institute of Physics, Pedagogical University, 30-084 Kraków, Poland
[3] Faculty of Computer Science, Electronics and Telecommunication, AGH University of Science and Technology, 30-059 Kraków, Poland
[4] Institute of Materials Science, Technische Universität Darmstadt, D-64287 Darmstadt, Germany
[5] Faculty of Mathematics and Physics, Charles University, Ke Karlovu 5, 12116 Prague, Czech Republic

E-mail: tarnawsk@up.krakow.pl and tarnawsk@mag.mff.cuni.cz

Received 7 March 2013
Accepted for publication 7 March 2013
Published 2 April 2013
Online at stacks.iop.org/ANSN/4/025004

Abstract
Multilayered thin films of Ti–TiO_2 system have been investigated, focusing on all of the important parameters in both photocatalysis and H storage. Numerous Ti–TiO_2 thin films with a single-, bi- and tri-layered structure have been deposited on different substrates by means of dc pulsed magnetron sputtering from a metallic Ti target in an inert Ar or reactive $Ar + O_2$ atmosphere. The film chemical composition, depth profile, layer thickness and structure were determined by combined analysis of x-ray diffraction, x-ray reflectometry, Rutherford back-scattering and optical reflectivity spectra. The results show that the Ti films deposited on Si(111) exhibit a strong preferred orientation with the (00.1) plane parallel to the substrate, while a columnar structure was developed for TiO_2 films. H charging at 1 bar and at 300 °C revealed that, in the case of the tri-layered structure of Ti/TiO_2/Ti/Si(111), H diffused through the TiO_2 layer without any accumulation in it. Pd acts as a catalyst for gathering H in Ti layers and up to 50% of H is stored in the topmost and bottom Ti layers. The preferential orientation in the Ti films was found to be destroyed upon hydrogenation at 100 bar. The hydride TiH_x phase ($x < 0.66$) was formed under such a high H pressure.

Keywords: titan oxides, multilayers, sputter, crystal structure, hydrogen storage

Classification numbers: 2.00, 5.00, 5.13

1. Introduction

Titanium dioxide (TiO_2) is one of the potential candidates for photocatalysts as it has the most efficient photoactivity, highest stability and lowest cost. Two types of photochemical reaction occur on a TiO_2 surface when irradiated with ultraviolet (UV) light: the first includes the photo-induced redox reactions of adsorbed substances and the other is the photo-induced hydrophilic conversion of TiO_2 itself. Recently, significant interest has been shown towards this material in newer fields such as homogeneous or heterogeneous catalysis. In fact, the beginning of a new era in heterogeneous photocatalysis was marked by the discovery by Fujishima and Honda in 1972 of the photocatalytic splitting of water on TiO_2 electrodes [1]. TiO_2 currently finds various novel applications in photoelectrochemistry, photocatalysis, solar cells and gas sensors [2–4]. In addition, there is at present great interest in H based energy. Thus, significant efforts have been focused on the use of photocatalysis for the light assisted production of H. This has led to intensive research, e.g. in the field of solar H (i.e. the photoelectrochemical splitting of water to produce gaseous H using solar energy). The pioneering work on solar H based on TiO_2 was published in the 1970s [1, 5]. However, even though the reaction efficiency is very high, TiO_2 can absorb only the UV light contained in the solar spectrum, which is only about 3%. The energy conversion efficiency (ECE) in the photoelectrochemical cell (PEC) was at the level of ∼0.5%. Thus the enthusiasm towards research into H_2

* Invited talk at the 6th International Workshop on Advanced Materials Science and Nanotechnology IWAMSN2012, 30 October – 2 November, 2012, Ha Long, Vietnam.

production waned in the middle of the 1980s and research shifted towards the utilization of the strong photo-produced oxidation power of TiO_2 for the destruction of pollutants. Recently, the wide-band gap semiconductor TiO_{2-x} (i.e. with a small departure ($x \neq 0$) from the stoichiometric composition) as well as the TiO_2-based materials are again being considered as the most promising candidates for photoelectrodes for solar H, where the search is focused on modifying properties to increase the ECE to the required level for commercialization[6, 7]. Moreover, the increased interest in TiO_2 is concerned with the development of its nanostructure forms, such as nanotubes and nanorods etc, for renewable energy sources and the H economy (e.g. H production, detection and even storage) [8–10]. For an extensive overview of the development of TiO_2 based photocatalysis and its future prospects from both scientific and technological viewpoints, see [11–13]. In particular, Fujishima *et al* [12] highlighted the astonishing number of publications involving heterogeneous photochemical studies (in general) and those specifically involving TiO_2: among about 2400 heterogeneous photochemistry papers published in 2008, roughly 80% involved TiO_2 based materials. During the last 10 years the number of papers published per year related to the use of TiO_2 for solar cells has increased steadily and reached more than 1000 in 2010 [14].

Ti itself and its alloys play an important role in many industrial applications (e.g. in aerospace, chemical processing and sports equipment) thanks to their excellent corrosion resistance and high specific strength. Besides, Ti is also known as a biocompatible element used successfully in body implants [15] due to its small atomic mass, good mechanical properties and harmless native oxide formed easily upon oxidation. Ti and its alloys have a high affinity for H; they can pick up a large amount of H up to more than 50 at.% H [16–18] at elevated temperatures above 600 °C (without the formation of a hydride phase). Thus they are considered to be promising materials for H storage applications which are a key enabling technology for the extensive use of H as an energy carrier (i.e. for the H economy). Besides, the hardness of Ti hydride was found to be about 30% higher than that of pure Ti [19].

Increasing interest has recently focused on the Ti–TiO_2 system, in particular on their application in the H economy. For example, TiO_2 nanotubes grown on Ti substrates by anodization may successfully be used for H storage [9]. Titanium hydride (TiH) films can be used as a neutron mirror, H storage layer and standard for H quantitative analysis. Saturation of these systems with H improves their reflectivity [20]. Metal–insulator–metal (MIM) structures such as Ti/TiO_2/Ti were proposed for resistance random access memory (ReRAM) [21, 22] because their resistance could be switched reversibly by an applied electric field. Understanding the structural and thermodynamic properties of Ti–TiO_2 systems, as well as their H absorption ability, is critical for the successful implementation of these materials. Although it is known that the diffusion of H in TiO_2 is slower than that in the pure metal, the mechanism by which the oxide influences H permeation into Ti and its alloys is still not well established [23, 24].

We are interested in the characterization of the thin film multilayer of a Ti–TiO_2 system prepared by reactive sputtering with the ultimate aim of investigating the interlayer properties and the influence of annealing, ion mixing and H intake on the microstructure and electronic structure. Numerous Ti–TiO_2 thin films with a single-, bi- and tri-layer structure deposited on different substrates by means of a dc pulsed magnetron sputtering technique were prepared and investigated. We first focused on the characterization of the as-sputtered films, such as chemical composition, film thickness and interface properties. Indeed the film thickness is a very important parameter in both photocatalysis and H storage. For instance, the photoactivity and photocatalytic activity of TiO_2 films deposited on soda-lime glass substrates by atomic layer deposition have been found to reach their maximum at a film thickness of 15 nm [25]. Application of H would affect the microstructure and properties of thin-film and multilayer structures. On the other hand, atom mixing and diffusion across the interfaces can also influence the H uptake. Thus selected multilayered Ti–TiO_2 films subjected to H charging at atmospheric pressure and/or at high pressures were then investigated, focusing on film stability, hydrogen uptake and H storage under different conditions.

2. Experimental set-up

The deposition process was carried out in a planar magnetron sputtering system described in detail elsewhere [26]. Magnetron discharge was driven by a dc pulse power supply. The target of 5 N Ti was sputtered either in high purity argon (for Ti layer deposition) or $Ar + O_2$ reactive gas atmosphere (for TiO_2 layer deposition). The sputtering rate of the target and the composition of the gas mixture were controlled by optical emission spectroscopy. The layer thickness was controlled by the deposition time. Substrates for film deposition were placed on a rotatable holder above the target at a distance of 35 mm. Up to eight samples could be obtained in one deposition cycle without breaking the vacuum thanks to a special construction of the shutter. The substrates prior to and during deposition were heated up to 250 °C. Films with different geometries (different layer structures) were deposited onto Si(111): (i) a single layer Ti/Si(111), (ii) a bi-layer TiO_2/Ti/Si(111) and (iii) a tri-layer Ti/TiO_2/Ti/Si(111). All of the layered structures were obtained under the same conditions by a simple switching between Ar and $Ar + O_2$ gas mixtures. The nominal thickness of each layer (d) was in the range of 10–250 nm, selected according to the different plans for investigations. For instance the thin films ($d = 10$–50 nm) were the subject of investigation of the layer quality. The thicker single-layer films ($d = 50$–250 nm) or the tri-layer films with similar (total) thickness were used for hydrogenation. One series of tri-layer films was subjected to an additional Pd covering. Namely, after Ti and TiO_2 layer deposition, they were partially (about a half of the film surface) covered by a 20 nm thick Pd layer by physical vapour deposition during which the layer thickness was controlled *in situ* using a quartz crystal microbalance.

For the measurements of the optical transmittance, some additional films with chosen parameters (e.g. with a similar thickness and layer structure as those deposited on Si substrates) were deposited onto amorphous silica transparent substrates. Selected films with a similar thickness

Table 1. The film geometry and the layer thickness (d (nm)) for different layers estimated by combined analysis (see text). The notation for single, bi- and tri-layered films deposited on Si(111) is respectively S (single), D (double) and T (triple). The additional letter 'C' indicates those deposited on C-foils, while those with '+Pd' denote the films covered partially by Pd. The number in parenthesis denote the layer sequence: Ti(1) is the first Ti layer deposited directly onto the Si(111) substrate and on C-foil; $TiO_2(2)$ is the second TiO_2 layer deposited onto the Ti(1) layer; and Ti(3) is the third Ti layer deposited onto the $TiO_2(2)$ layer. The additional Pd layer was deposited onto about half of the surface of the two films (Pd (partial)) used for investigation of hydrogenation. Films used for the hydrogenation at 1 bar and at high pressures are marked by (*) and (**), respectively.

		Layer thickness d (nm)			
Notation	Film geometry	Ti(1)	$TiO_2(2)$	Ti(3)	Pd
S1	Ti/Si(111)	47			
S2	Ti/Si(111) **	67			
S3	Ti/Si(111) **	240			
D1	TiO_2/Ti/Si(111)	46	46		
D2	TiO_2/Ti/Si(111)	100	110		
D3 + Pd (partial)	Pd/TiO_2/Ti/Si(111) *	79	97		20
D4	TiO_2/Ti/Si(111)	100	160		
D4-C	TiO_2/Ti/C-foil	100	160		
D5	TiO_2/Ti/Si(111) **	15	60		
T1	Ti/TiO_2/Ti/Si(111)	49	51	40	
T2	Ti/TiO_2/Ti/Si(111)	100	110	50	
T3 + Pd (partial)	Pd/Ti/TiO_2/Ti/Si(111) *	80	96	40	19
T4	Ti/TiO_2/Ti/Si(111)	100	150	120	
T4-C	Ti/TiO_2/Ti/C-foil	100	150	120	
T5	Ti/TiO_2/Ti/Si(111) **	15	60	20	

were also deposited on C-foils. The O signal in the films deposited on C-foils appeared as a well-separated peak in the Rutherford back-scattering spectra. Thus the O content can be analysed in more detail in those films and would give additional supporting information for the films deposited on Si substrates.

Two series of tri-layer films (with and without Pd cover) were charged with H at the same temperature (300 °C) and pressure (1 bar), but for different times. Two other series of single- and tri-layer films were hydrogenated at high H pressure of up to 102 bar at room temperature and at different times.

The film chemical composition, depth profile, layer thickness and structure were determined by combined analysis of x-ray diffraction (XRD), x-ray reflectometry (XRR), Rutherford back-scattering (RBS) and optical reflectivity spectra. For data evaluation of the RBS spectra, the computer code SIMNRA [27] was used and the simulated areal density value was converted into the layer thickness in nm, so that it can be compared with the (thickness) value estimated from other methods. Details of our RBS analysis, in particular the conversion of the RBS layer thickness into nm, has been described elsewhere [28, 29]. The film geometry, estimated layer thickness and film notations of different films used in the experiments are given in table 1.

The electrical resistivity was measured using the four point method for the films on hydrogenation at different steps. The applied current was in the range of 1–100 mA. Cross-section and surface images were obtained by scanning electron microscopy (SEM) for thin films using a Hitachi SU-70 apparatus and/or Philips XL 30 FEG microscope.

The H profile was determined by means of a secondary ion mass spectroscopy (SIMS) and N-15 nuclear reaction analysis (^{15}N-NRA method). SIMS was carried out using Cs^+ primary ions recording positive secondary ions by a CAMECA ims 5f equipment. The reaction $^{15}N + {}^{1}H \rightarrow {}^{12}C + \alpha + \gamma$ (4.965 MeV) (i.e. the reaction $^{15}N(p, \alpha\gamma)^{12}C$ revealed by the specific 4.965 MeV γ-rays of the ^{12}C) at a resonance energy of 6.417 MeV was used for the ^{15}N-NRA method to obtain the results. For data evaluation the computer code SRIM was used. More details of these experiments have been reported previously [30, 31].

3. Results and discussion

3.1. The as-sputtered films

XRD patterns of the deposited layered structures: Ti/Si(111), TiO_2/Ti/Si(111) and Ti/TiO_2/Ti/Si(111) with a nominal thickness of 50 nm are shown in figure 1 (left panel). For a comparison, the XRD pattern for a single layer of Ti deposited onto amorphous silica SiO_2, i.e. Ti/SiO_2 with a similar thickness, is also given in the same figure. The intensity of all Ti diffraction lines is very small except for the peak corresponding to the (10.3) crystallographic plane and their widths are quite broad ($> 1^\circ$). The results revealed that the Ti films, crystallizing in the hexagonal structure, exhibit a strong preferred orientation with the (00.1) plane parallel to the substrate [30] (i.e. the c-axis of the hexagonal cell of Ti crystallites is perpendicular to the substrate). We notice here that the observed preferential orientation of Ti crystallites is not forced by the substrate Si(111), since it is preserved even in the uppermost Ti layer deposited on the TiO_2 layer of a triple structure of Ti/TiO_2/Ti. Such a preferential growth of the Ti layer can be observed even in the case of film deposition on amorphous silica SiO_2 substrate. The presence of TiO_2 of the rutile polymorphic form can be detected in the XRD patterns of the bilayer film TiO_2/Ti/Si(111), indicated by $TiO_2(110)$, $TiO_2(211)$ and $TiO_2(200)$ reflection. All these reflections are quite visible when TiO_2 is the uppermost layer in the structure. When the (additional) Ti layer was deposited on top of the TiO_2 layer, all those peaks disappear except for the strongest $TiO_2(110)$ one revealed as a broad bump around $2\theta = 27^\circ$. However, for such a trilayer Ti/TiO_2/Ti

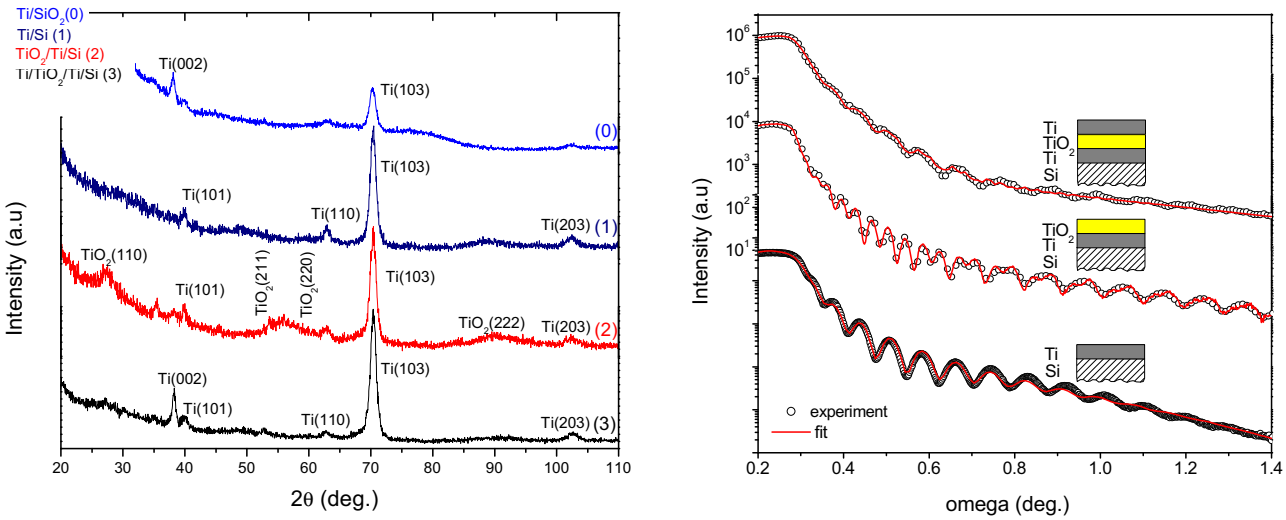

Figure 1. XRD pattern (left) and XRR curves (right) for Ti/Si(111), TiO_2/Ti/Si(111), Ti/TiO_2/Ti/Si(111) film with the layer thickness of each layer at about 50 nm (sample S1, D1, T1 in table 1). The XRD pattern of the Ti/SiO_2 film is shown for comparison. The layer structure of the films used for XRR fitting is also labelled. The curves were shifted as a guide for the eye.

film, the Ti(002) reflection become dominant. Indeed this reflection is the second strongest one in the XRD pattern for the tri-layer film. Such Ti(200) reflection is also very visible for the single layer Ti film deposited on the SiO_2 substrate. The XRR curves for those three films deposited on Si(111) are shown in figure 1 (right panel). In all cases, quite reasonable fits to the experimental data were obtained. XRR data analysis revealed that the film density is 4.57–4.62 g/cm^{-3} for Ti (i.e. close to the bulk value) and 3.72–4.07 g/cm^{-3} for TiO_2 (lower than the bulk value). The interface roughness is found to be of the order of 1.3–3.2 nm, which is typical for samples grown by magnetron sputtering [30].

The measured and simulated RBS spectra of these three samples are shown in figure 2. A large Ti-peak related to the backscattered signal from the first Ti layer deposited on the Si(111) substrate (denoted as the Ti(1) layer) was observed at energy of about 1400 keV. The backscattered signal from the TiO_2 layer deposited on top of the Ti(1) layer (TiO_2(2) layer) leads to the appearance of a shoulder on the right hand side of the Ti(1)-peak and a widening of the Ti peak as well as a visible O peak around 700 keV. In the case of the tri-layer film, a double maxima feature and a doubled peak width were observed in the energy range of 1300–1500 keV, as a result of the backscattered signal from the Ti layer (Ti(3) layer, the surface layer) deposited onto the TiO_2 layer. The layer thicknesses of the Ti layers are similar (see table 1), and the intensities of the two maxima are quite similar. The RBS analysis shows that for all films with different layer geometries (i.e. with single, bi- and tri-layers), there is no Ti interdiffusion (within the RBS error limit) from the first Ti layer into the Si substrate, and thus a sharp interface was always obtained. Some small interdiffusion can be seen at the Ti–TiO_2 interface for the bi-layer film and at both Ti–TiO_2 and TiO_2–Ti interfaces of the tri-layer film. However, since we use standard RBS, it would be ambiguous to discuss the (interface) layer with a thickness of several nanometres. The combined analysis of RBS, XRD and XRR indicate the real thickness of each layer to be less than the nominal one (see table 1).

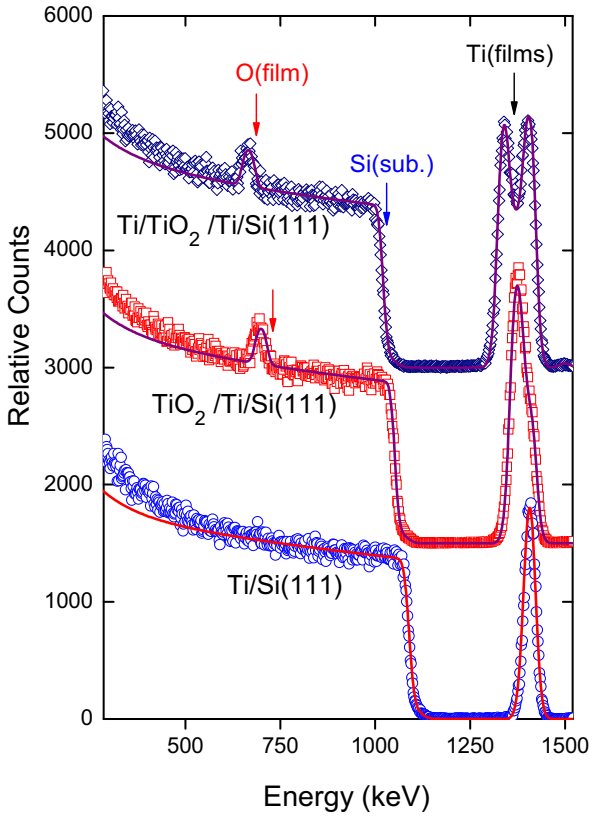

Figure 2. Random RBS (markers) and SIMNRA (lines) simulated spectra for Ti/Si(111), TiO_2/Ti/Si(111) and Ti/TiO_2/Ti/Si(111) film with the layer thickness of each layer at about 50 nm (sample S1, D1, T1 in table 1). The curves were shifted as a guide for the eye. The arrows mark the Ti and O signals in the films (Ti(films), O(film) and the Si signal from the substrate (Si(sub.)). RBS experiments were performed with a 2 MeV He^+ ion beam and a backscattering angle of 171°.

We performed BRS measurements on different films with different geometries and layer thicknesses. The change/development of Ti, O and Si signals for selected films is shown in figure 3. For the single-layered films, a single

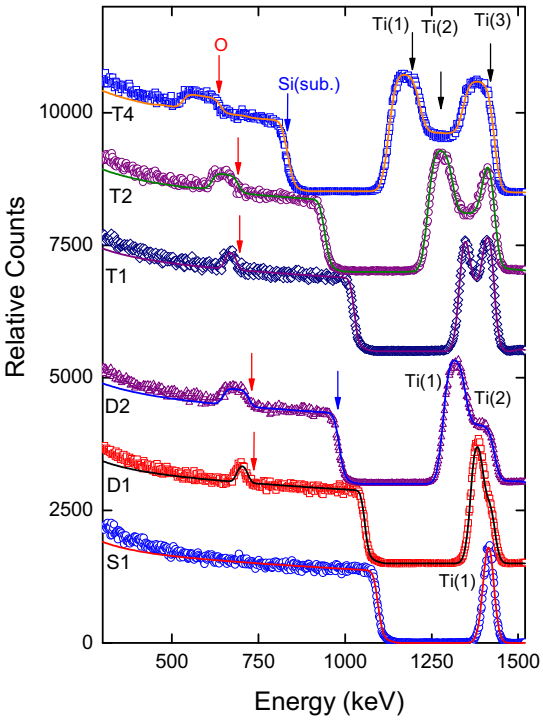

Figure 3. The change/development of Ti, O and Si signals in RBS spectra with changing film geometry and layer thickness. The random and SIMNRA simulated RBS spectra are shown by markers and solid lines, respectively. The sample notation and layer thickness are given in table 1. The curves have been shifted as a guide for the eye. The arrows mark the Ti- and O signals in the films and the Si signal from the substrate. Ti (1): the Ti layer deposited directly on the Si substrate. Ti(2): the TiO_2 layer deposited on the Ti(1) layer. T(3): the Ti layer deposited on the TiO_2 layer. RBS experiments were performed with a 2 MeV He^+ ion beam and a backscattering angle of 171°.

sharp Ti peak is always observed. Increasing the thickness of the Ti(1) layer leads only to an increase of the width and intensity of the Ti(1) peak and a shift of the Si-edge to lower energies. For the bi-layer films, introduction of the TiO_2(2) layer leads to the appearance of the O signal revealed by the distinct peak in the high 'background' signal from the Si substrate. The shoulder-like feature in the Ti peak appeared for the films with a layer thickness of below 50 nm (i.e. sample D1). With increasing thickness of the TiO_2(2) layer, the shoulder changes into a plateau as a result of a large widening of the signal coming from such a layer (the Ti(2) signal). From our more detail investigation of the shape of the RBS spectra as a function of the layer thickness, we found out that the plateau figure becomes visible for TiO_2(2) layer thicknesses $>$ 100 nm (e.g. sample D2). For the tri-layer films, the double maxima are always observed to be related to Ti signals. The intensity and width of these double maxima increase with increasing layer thickness, while the minimum between them is governed by the Ti(2) signal in the TiO_2 layer. Obviously, a similar intensity and width of the two maxima was obtained for the films in which the layer thickness of the Ti(1) and Ti(3) layer is similar (i.e. samples T1 and T4). In all cases, increasing the total film thickness implies a widening of the O signal and a shift of the Si edge to lower energies.

The introduction of the TiO_2 layer into the bi- and tri-layered films deposited on the Si(111) substrate leads to the appearance of the O signal, which is revealed by the distinguished peak on the high background signal from the Si substrate. It is related to the fact that the atomic mass of O (16) is smaller than that of Si (28) and thus the energy of scattered He^+ ions from the O atoms in the films is always smaller than that from the Si atoms in the substrates. Thus for these films the uncertainty is very high for fitting the data below the Si edge, i.e. in the energy region where the O and Si signals are combined. For more precise analysis of the O signal (and thus better fits of the RBS spectra), we prepared two film series with similar layer thickness and film geometry, one on Si(111) substrates and the other one on C-foil. The atomic mass of O (16) is bigger than that of C (12). Thus the O signals from the films will appear separately in the RBS spectra, i.e. at energy higher than that of the C edge coming from the C substrate. The O concentration can be then analysed in more detail in those films and can give additional supporting information for the films deposited on Si substrates. Comparison of the measured and simulated RBS spectra of selected bi- and tri-layered films deposited on Si(111) and C foil is shown in figure 4. The thickness of each layer was chosen in the range of 100–150 nm (samples D4, D4-C, T4 and T4-C in table 1). Indeed, the determination of layer thickness and element concentration by means of SIMNRA simulation performed on the films deposited on the C-foil seems to be simpler, due to the fact that the O signal appears as a broad peak on the zero-background, as expected. However, while there is almost no interdiffusion in the films deposited on Si(111) substrates, C diffusion (up to 10%) into the film was observed. If the films are thin (layer thickness $<$ 30 nm), the C can be found even in the surface layer. Since no C was detected in the surface layer for the thick films (no C surface contamination) with film thicknesses $>$ 100 nm, we assume that the C on the surface of the thin film was due to C segregation from the substrates.

3.2. Hydrogen profiling

We have characterized H absorption by Ti and TiO_2 films in the Ti–TiO_2 system under H charging under a pressure of 1 bar with specific emphasis on H diffusion and its storage in each layer [31].The films were charged for different times and at temperature of 300 °C. The focus of this aspect of the study were the films with the notations D3 + Pd and T3 + Pd in table 1. Since about a half of the film surface was covered by an additional Pd layer, this allows us to simultaneously investigate the H charging in similar films without and with Pd cover. Prior to the other experiments the film composition and thicknesses were studied by RBS. The experiments were performed on both the areas with Pd and without Pd covering on the films. Besides signals from the backscattering of He^+ ions on Ti, O and Si atoms, a sharp peak revealing the binary elastic collision of He^+ ions on Pd atoms was observed, shown in figure 5. The thickness of the Pd layer is 19–20 nm (see table 1), i.e. nominal thickness as expected. The RBS analysis indicates that there is no interdiffusion at the interfaces, in good agreement with the SEM image revealing a smooth and homogenous surface layer with a sharp borderline between the Ti surface layer and the Pd layer [30].

We focused on the H profiling of the tri-layer films, and compared the results obtained for the film areas with and

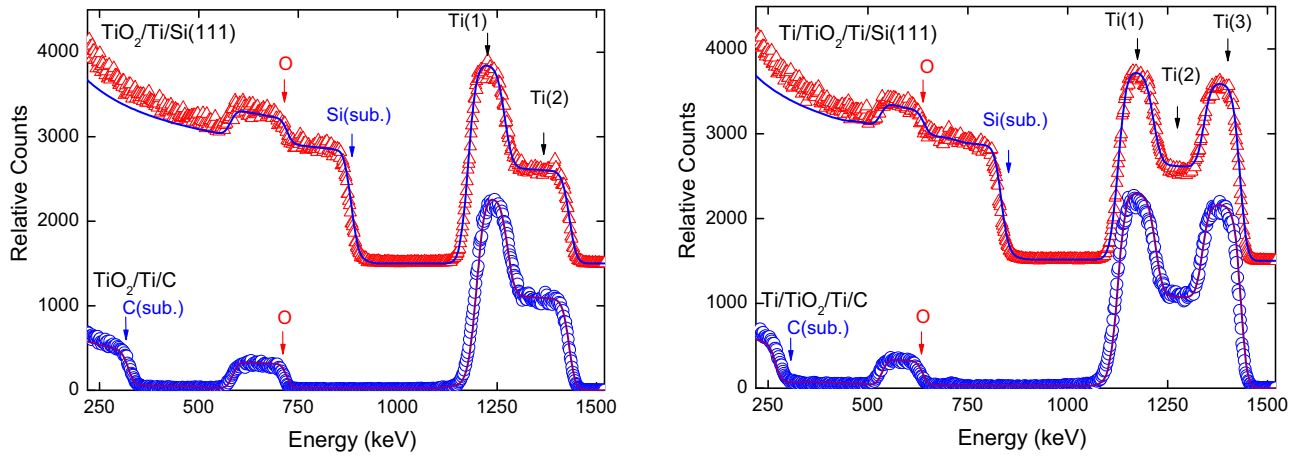

Figure 4. Random RBS (markers) and SIMNRA (lines) simulated spectra for $TiO_2/Ti/Si(111)$ and $TiO_2/Ti/C$-foil (left) and $Ti/TiO_2/Ti/Si(111)$ and $Ti/TiO_2/Ti/C$-foil (right); samples D4, D4-C, T4 and T4-C in table 1. The arrows mark the Ti- and O signals in the films and the Si or C signal from the substrate (S(sub.), C(sub.)). RBS experiments were performed with a 2 MeV He^+ ion beam and a backscattering angle of 171°.

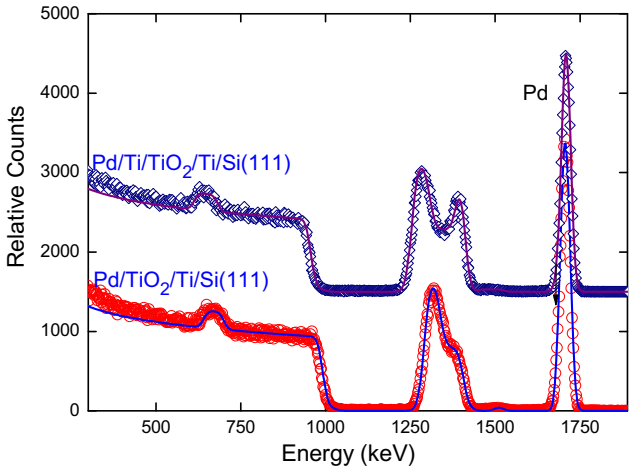

Figure 5. Random RBS (markers) and SIMNRA (lines) simulated spectra for $TiO_2/Ti/Si(111)$ and $Ti/TiO_2/Ti/Si(111)$ films covered by 20 nm thick Pd layer used for H charging experiments (samples D3 + Pd. T3 + Pd in table 1). The Pd signal was indicated by the sharp peak at around 1.7 MeV. RBS experiments were performed with a 2 MeV He^+ ion beam and a backscattering angle of 171°.

without Pd covering. The H profiles determined from SIMS and ^{15}N-NRA are shown in figures 6 and 7. Prior to the H charging of the films, a small amount of H was revealed by the SIMS measurements to be coming from H absorption of the film surface. In the films without Pd (sample T3), charging with H increased the H amount in the top Ti layer (Ti(3) layer) significantly. However, in the bottom Ti layer (i.e. the Ti(1) layer deposited onto the Si substrate) the concentration of H remains very low. In the film covered by Pd (sample T3 + Pd), the H concentration in the top Ti layer (Ti(3) layer) was enhanced significantly after charging with H, similar to the film without Pd cover. In essence, the existence of the Pd top layer leads to an enormous amount of H in the bottom Ti layer. In both cases, little change was observed in the TiO_2 layer, i.e. the H concentration in the TiO_2 layer remained the same as before.

The ^{15}N-NRA indicates that for the $Ti/TiO_2/Ti/Si(111)$ film, the accumulation of H in the top Ti layer can be up to 40% , while it amounts to only 15% in the bottom Ti layer for the $Ti/TiO_2/Ti/Si(111)$ film. For the $Pd/Ti/TiO_2/Ti/Si(111)$ film, the accumulation of H in the top Ti layer is higher, up to 50%. The measurements revealed a lack of H in the Pd layer. However, a Pd layer on top of a Ti layer results in a large enhancement of the H amount in the bottom Ti layer: a total amount of H with a concentration of about 50% was achieved in the Ti(1) layer, i.e. almost the same as that in the top Ti(3) layer. In addition, a large amount of H was found throughout all of the Ti (1) films. Thus Pd would appear to promote H penetration into Ti. In both cases, in the oxide layer H only amounts to less than 5%. These ^{15}N-NRA results are in a good agreement with those from the SIMS measurements, indicating that Pd acts as a catalyst for gathering H in Ti layers [31]. We assume that Pd facilitates the dissociation of H molecules at its surface. When Pd metal atoms are on the surface, they can promote the dissociation of H molecules and so the H atoms can easily be absorbed by the bulk of the metal and diffuse through other layers.

One surprising fact was that H diffuses through the TiO_2 layer without any accumulation there, both for the films with and without Pd cover. We assume that the mechanism proposed by Bates *et al* [32] also works in our case. Namely, the diffusion of H and its isotopes through a TiO_2 sample can occur in both the directions parallel and perpendicular to the *c*-axis. However, due to the large open channels parallel to the *c*-axis, diffusion of H is faster in this direction and proceeds by a proton jump from one O_2 ion to another along this channel. In fact, SEM cross-sectional images of the tri-layer films [30] revealed the columnar structural growth of TiO_2 layers on the bottom Ti film and thus large channels for H diffusion are found to be parallel to the *c*-axis.

3.3. Influence of hydrogenation on the film crystallinity

The hydrogenation at high pressures was performed on the single and tri-layer films; the S2, S3, D5 and T5 samples in table 1. Figure 8 (left panel) shows the XRR curves of the single layer S2 upon hydrogenation at two different H pressures. A quite reasonable fit to the experimental

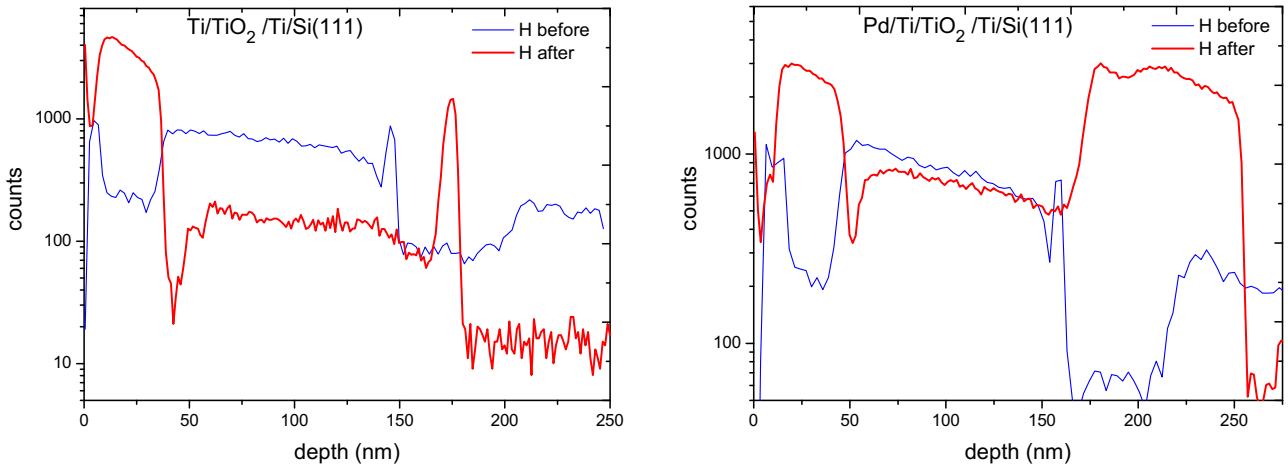

Figure 6. Comparison of the H profile determined by SIMS for the $Ti/TiO_2/Ti/Si(111)$ film (left, sample T3) and $Pd/Ti/TiO_2/Ti/Si(111)$ film (right, sample T3 + Pd) before and after H charging at 1 bar and at a temperature of 300 °C.

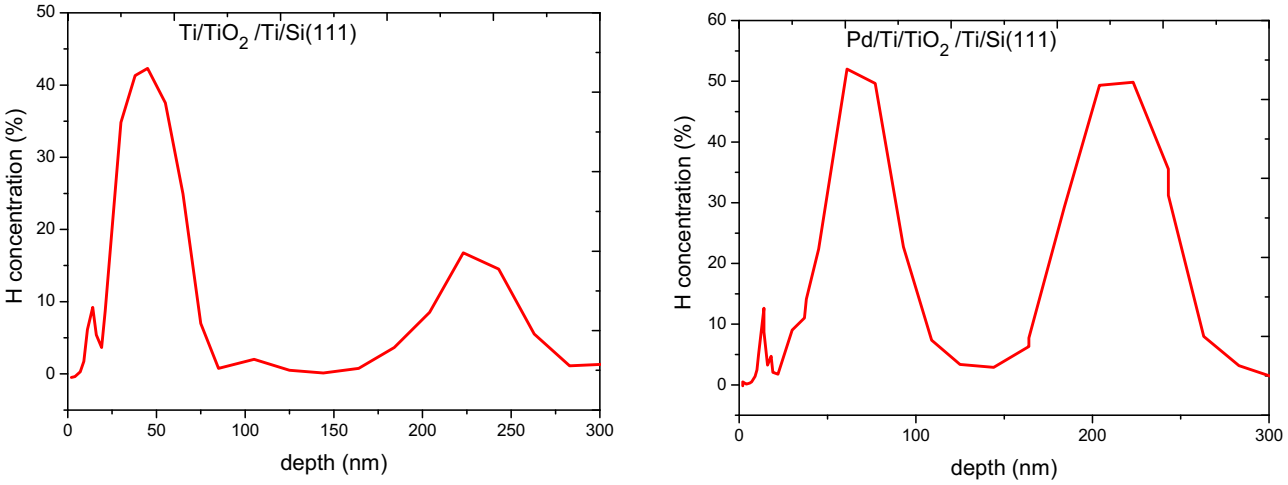

Figure 7. Comparison of the H profile determined by ^{15}N-NRA for the $Ti/TiO_2/Ti/Si(111)$ film (left, sample T3) and $Pd/Ti/TiO_2/Ti/Si(111)$ film (right, sample T3 + Pd) after H charging at 1 bar and at a temperature of 300 °C

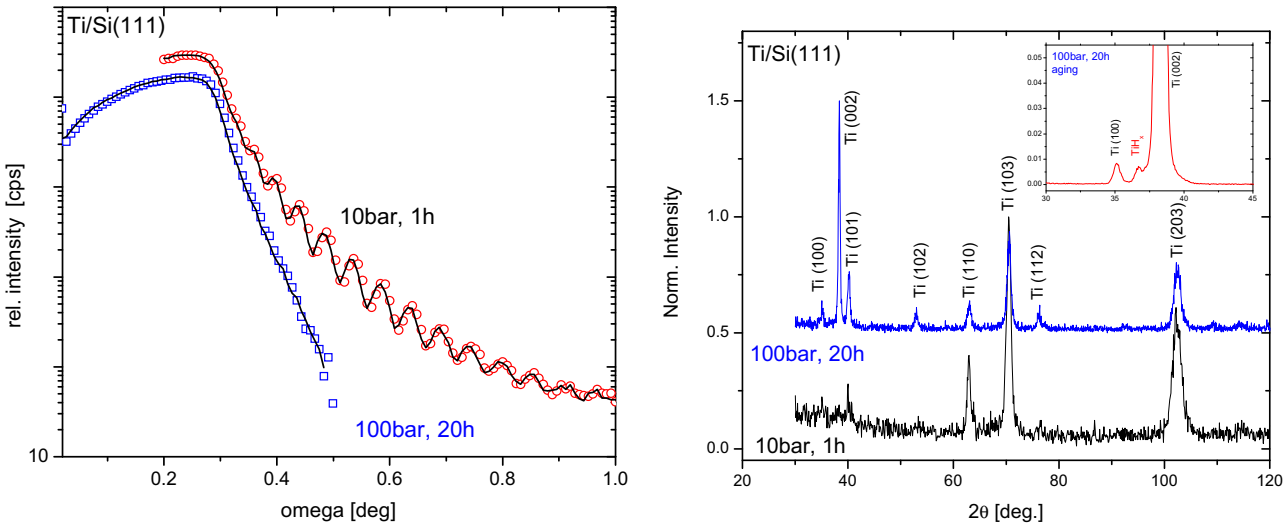

Figure 8. The XRD pattern (left) and XRR curves (right) for a 67 nm Ti/Si(111) film (sample S2) upon hydrogenation at 10 bar for 1 h and at 100 bar for 20 h and at room temperature. The curves were shifted as a guide for the eye. Inset: the XRD pattern of the film after hydrogenation at 100 bar for 20 h performed on the film after 10 months revealing the TiH_x phase.

data was obtained (the model of a single layer requires five fitting parameters of which the most important are its thickness and density as well as the interface roughness). The estimated value for the thickness was 67 nm in this case, a little higher than the nominal thickness. The XRR results revealed that the layer structure of the film is still very good upon hydrogenation at a pressure of H_2 gas of $p_{H2} = 10$ bar. The periodicity of the XRR curve was similar to that of the as-deposited film. Increasing hydrogenation pressure to 100 bar leads to a disappearance of the periodicity of the XRR curve. A similar thickness was found for the hydrogenated film (S2) at 100 bar, indicating no visible swelling effect. However, hydrogenation causes an increase of the layer roughness. Namely, a roughness value (r) of 1.8 and 3.6 nm was estimated for the film after hydrogenation at $p_{H2} = 10$ and 100 bar, respectively. In other words, the sample after hydrogenation at 100 bar has become much rougher and this can explain why the Kiesieg fringes in XRR have disappeared. We note here that the film roughness of the as-deposited films was in the range of 1.0–1.3 nm [30] and no visible difference in the film roughness was found for the film upon H charging at 1 bar and at a temperature of $T = 300\,^{\circ}$C ($r = 1.1$ nm) [31]. Figure 8 (right panel) shows the XRD pattern of the 67 nm Ti/Si(111) film (S2) after hydrogenation. For a comparison of the relative change in the peak intensity of different reflections, each XRD pattern was normalized so that the most intense diffraction line was set to 1 (the Ti(103) reflection for different films at 0 and at 10 bar and the Ti(002) reflection for those at 100 bar). Individual diffraction patterns were then shifted vertically with respect to each other. Similar to the other studied single films, the intensity of all of the diffraction lines of the as-deposited film is very small, except for the peak corresponding to the (10.3) crystallographic plane. It confirmed a strong preferred orientation (with the (00.1) plane parallel to the substrate) in the Ti layer. For hydrogenation at 10 bar, a large enhancement of the Ti(203) and Ti(110) peaks was observed with the intensity reaching 60 and 40%, respectively, with respect to that of the Ti(103) reflection. The diffraction peaks are quite broad ($> 1^{\circ}$), in particular the Ti(203) one. A very similar XRD pattern was also observed for the thicker film (sample S3) of 240 nm Ti/Si(111) upon hydrogenation under the same conditions. As pointed out previously [30], the preferential orientation of Ti crystallites is not forced by the substrates and thus it would not be influenced by the film thickness. When increasing H pressure to 100 bar, many more Ti peaks appeared. Moreover, the Ti(002) peak becomes most intense; its intensity is two times larger than that of Ti(103). The results indicate that hydrogenation at high pressures ($p_{H2} =$ 100 bar) destroys the preferential orientation of the Ti film and thus the situation returns to normal, exhibiting the standard XRD pattern. We note here also that no peak shift and no peak widening were observed for any peak. This indicates that a large absorption of H in this thin Ti film ($d = 67$ nm) does not lead to any (visible) lattice expansion. In other words, no visible swelling effect was observed. This is in a good agreement with XRR data (revealing a similar film thickness before and after hydrogenation). We recall here the disappearance of the XRR periodicity of this thin film under hydrogenation at 100 bar. This would also be consistent

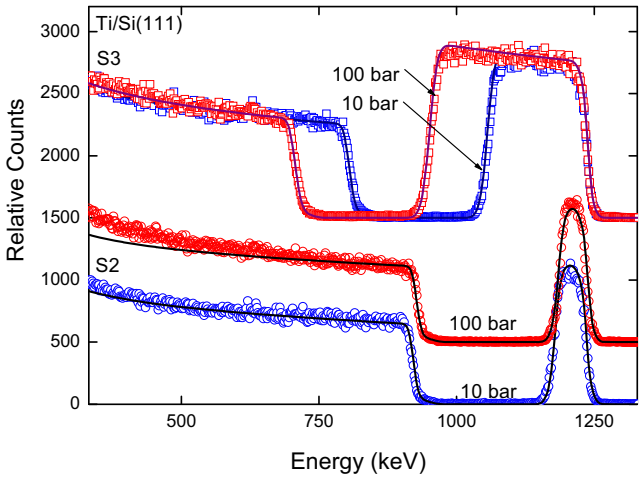

Figure 9. Random RBS (markers) and SIMNRA (lines) simulated spectra for hydrogenated single layer Ti/Si(111) films (S2, S3 in table 1) at 10 and 100 bar. RBS experiments were performed with a 1.7 MeV He^+ ion beam and a backscattering angle of 171°.

with the XRD data, which reveals that the film becomes better crystallized and the crystallites become bigger and protrude from the surface causing the increase of roughness. The titanium hydride phases TiH_x, e.g. titanium dihydride ($x = 2.0$), could be formed under such a high H pressure. However, the reflections of such hydride phases are very close to those of Ti. Therefore, we cannot rule out the existence of TiH_x phases in the film. We performed glancing incidence x-ray diffraction (GIXD) on this film. Very low intensity was observed in GIXD, revealing a high texture of Ti in the film. The film after hydrogenation at 100 bar was re-measured after 10 months. It is significant that we observed in this case that an additional reflection located at $2\theta = 36.7^{\circ}$ contributed to the TiH_x phase (with $x < 0.66$).

RBS measurements were performed on these hydrogenated films, shown in figure 9. The RBS analysis for a single thin Ti film (S2) confirmed that no swelling effect was observed, i.e. there was no visible change in the film thickness. However, for the hydrogenated film at 10 bar, we were easily able to fit the measured RBS spectra with one Ti layer and without any diffusion and without using the 'roughness' option from the SIMNRA simulation. For the data at 100 bar, although we could find a similar film thickness from the width of the Ti peak, it was difficult to get a good overall fit even when (partially) using the roughness option. We present the data for 100 bar in the same figure, in order to point out that a similar peak width was observed for the Ti peak at both 10 and 100 bar. However, the small difference between these two films cannot easily be seen, except that the simulated spectrum is very well fitted to the data for the film at 10 bar for the whole energy range even if at a low energy region, while a good fit was obtained for those at 100 bar only down to around 750 keV. We suggest the reason for this is the fact that the roughness is increased, as seen in the XRR, and the thus the film is far from ideal for RBS analysis. In other words, the RBS data also supported the XRR finding. No visible swelling effect from hydrogenation at 102 bar was observed for sample D5, since the film is still thin (with a total thickness of 75 nm). A large swelling effect was observed for the thick Ti film ($d = 240$ nm, sample

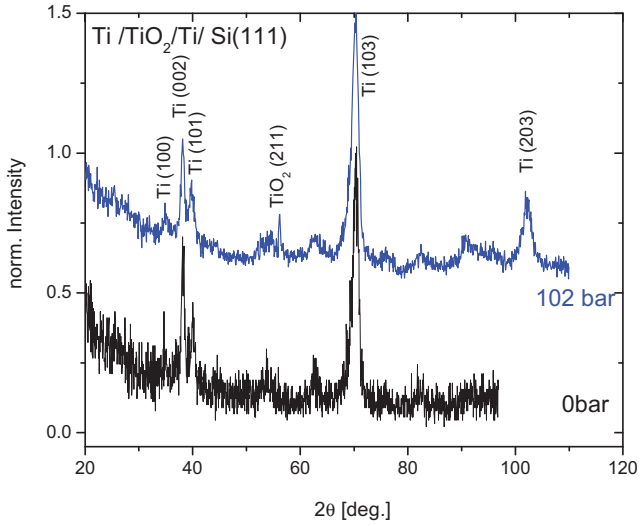

Figure 10. Comparison of the x-ray diffraction patterns for tri-layer film $Ti/TiO_2/Ti/Si(111)$ (sample T5) after hydrogenation at 102 bar for 20 h with that before hydrogenation (as-deposited film). The curves were shifted as a guide for the eye.

S3). Surprisingly in this case, we could easily find a good simulated RBS fit even if after hydrogenation at 102 bar using just a single layer. The thickness value after hydrogenation at 10 bar is almost the same ($d = 240$ nm), but it amounts to 370 nm after hydrogenation at 100 bar, i.e. the thickness increased by more than 150%.

The effect of hydrogenation on the crystal structure of the tri-layer film (sample T5) is shown in figure 10. In the as-deposited state, unlike the single layer film, except for the intense Ti(103) reflection, Ti(002) and Ti(101) were also observed. The appearance of the Ti(002) reflection in the tri-layer film has been reported previously [30]. Hydrogenation at $p_{H2} = 102$ bar generally did not lead to a visible change of the XRD pattern except for the fact that all reflections became more visible. In addition, an additional peak was observed at 54° which contributed to the rutile phase, i.e. $TiO_2(211)$ reflection. Since the total film thickness is only 95 nm in which the total thickness of the Ti layers is only 35 nm, we did not expect to observe any swelling effect in this case. (The H can be stored in Ti layers but barely any remains in the TiO_2 layer). The RBS measurements did indeed confirmed this. Namely, no change in the film thickness upon hydrogenation was revealed for the tri-layer film.

4. Summary

The main outcomes of our investigations of numerous thin films of Ti–TiO_2 system with different film geometry and layer thickness are summarized as follow.

1. The thin films of the Ti–TiO_2 system deposited by magnetron sputtering onto Si(111) substrates revealed that there is no Ti interdiffusion from the first Ti layer into the Si substrate. There is some minor interdiffusion at the Ti–TiO_2 interface for the bi-layer films and at both the Ti–TiO_2 and TiO_2–Ti interfaces of the tri-layer film. This may be related to the intergrowth between the Ti and TiO_2 layers, most probably due to the columnar structural growth of TiO_2.
2. Pd acts as a catalyst for H diffusion in the Ti layers. A great enhancement of H storage in the films (with a maximum concentration of H up to 50%) was obtained by introducing an additional thin Pd layer on top of the Ti–TiO_2 system.
3. H can diffuse through the TiO_2 layer without any accumulation there. Such a phenomenon is most probably related to the columnar structure of TiO_2.
4. The preferential orientation in the Ti films (with the *c*-axis of the hexagonal cell of Ti crystallites perpendicular to the substrate) was removed upon hydrogenation at high pressures ($p_{H2} = 100$ bar).
5. For the thin Ti films ($d < 100$ nm) and for the thick film ($d = 240$ nm), the film thickness did not change much upon hydrogenation at 10 bar. A large swelling effect was observed for the thick Ti layer upon hydrogenation at 100 bar. The significant H storage can increase the film thickness by 150%.

Acknowledgments

The authors gratefully acknowledge the financial support from the Foundation for Polish Science MPD Programme, co-financed by the EU European Regional Development Fund, project NN 515 080637 for Science in 2009–2012, the DAAD project D/08/07729 and the MNiSW project Nr 651/N-DAAD/2010/0. The authors thank J Gassmann, S Flege, C Schmitt (Institute of Materials Science, TU Darmstadt), D Rogalla, H-W Becker (Dynamitron Tandem Lab, Ruhr-Universität Bochum), M Perzanowski and M Marszałek (Institute of Nuclear Physics, Polish Academy of Sciences) for their valuable help with the experiments. Most of the experiments were performed in Krakow, Darmstadt and Prague in the framework of the authors' international cooperation projects. Some specific measurements were carried out at partner institutions (e.g. SEM by Hitachi apparatus at the Institute of Physics in Warszaw, NRA at the Dynamitron Tandem Laboratorium of Ruhr-Universität Bochum).

References

[1] Fujishima A and Honda K 1972 *Nature* **238** 37
[2] Linsebigler A L, Lu G and Yates J T Jr 1995 *Chem. Rev.* **95** 735
[3] Grätzel M and O'Regan B 1991 *Nature* **353** 737
[4] Varghese O K and Grimes C A J 2003 *Nanosci. Nanotechnol* **3** 277
[5] Fujishima A, Kohayakawa K and Honda K 1975 *J. Electrochem. Soc.* **122** 1487
[6] Murphy A B, Barnes P R F, Randeniya L K, Plumb I C, Grey I E, Horne M D and Glasscock J A 2006 *Int. J. Hydrogen Energy* **31** 1999
[7] Nowotny J, Bak T, Nowotny M K and Sheppard L R 2007 *Int. J. Hydrogen Energy* **32** 2609
[8] Lim S-H, Luo J, Zhong Z, Ji W and Lin J 2005 *Inorg. Chem.* **44** 4124
[9] Pillai P, Raja K S and Misra M 2006 *J. Power Sources* **161** 524
[10] Ni M, Leung M K H, Leung D Y C and Sumathy K 2007 *Renewable Sustainable Energy Rev.* **11** 401

[11] Hashimoto K, Irie H and Fujishima A 2005 *Japan. J. Appl. Phys.* **44** 8269
[12] Fujishima A, Zhang X and Tryk D A 2008 *Surf. Sci. Rep.* **63** 515
[13] Henderson M A 2011 *Surf. Sci. Rep.* **66** 185
[14] Baraton M-I 2011 *Open Nanosci. J.* **5** 64
[15] Niinomi M 2002 *Metall. Mater. Trans.* **33A** 477
[16] Numakura H and Coiwa M 1984 *Acta Metall.* **32** 1799
[17] Woo G C, Weatherly C E, Coleman C E and Gillbert R W 1985 *Acta Metall.* **33** 1897
[18] Tal-Gutelmacher E and Eliezer D 2004 *Mater. Trans.* **45** 1594
[19] Xu J J, Cheung H Y and Shi S Q 2007 *J. Alloys Compounds* **436** 82
[20] Maaza M, Jiang Z, Samuel F, Farnoux B and Vidal B 1992 *J. Appl. Crystallogr.* **25** 789
[21] Choi B J *et al* 2005 *J. Appl. Phys.* **98** 033715
[22] Kim W-G and Rhee S-W 2010 *Microelectron. Eng.* **87** 98
[23] Pound B G 1991 *Corrosion* **47** 99
[24] Pyun S I, Park J W and Yoon Y G 1995 *J. Alloys Compounds* **231** 315
[25] Kääriäinen M-L, Kääriäinen T O and Cameron D C 2009 *Thin Solid Films* **517** 6666
[26] Brudnik A, Czternastek H, Zakrzewska K and Jachimowski M 1991 *Thin Solid Films* **199** 45
[27] Mayer M 1999 *AIP Conf. Proc.* **475** 541; SIMNRA (Simulation Program for the Analysis of NRA, RBS and ERDA) developed by M. Mayer; http://www.rzg.mpg.de/_mam/
[28] Kim-Ngan N-T H, Balogh A G, Meyer J D, Brötz J, Hummelt S, Zając M, Ślęzak T and Korecki J 2008 *Surf. Sci.* **602** 2358
[29] Kim-Ngan N-T H, Balogh A G, Meyer J D, Brötz J, Zając M, Ślęzak T and Korecki J 2009 *Surf. Sci.* **603** 1175
[30] Drogowska K, Tarnawski Z, Brudnik A, Kusior E, Sokołowski M, Zakrzewska K, Reszka A, Kim-Ngan N-T H and Balogh A G 2012 *Mater. Res. Bull.* **47** 296
[31] Drogowska K, Flege S, Schmitt C, Rogalla D, Becker H-W, Kim-Ngan Nhu-T H, Brudnik A, Tarnawski Z, Zakrzewska K and Balogh A G 2012 *Adv. Mater. Sci. Eng.* **2012** 269603
[32] Bates J B, Wang J C and Perkins R A 1979 *Phys. Rev.* B **19** 4130